ACS OMEGA

http://pubs.acs.org/journal/acsodf
Article

Computational Investigation of a CO_2 Conversion Strategy via Diels–Alder Reaction in a Carbon Capture Solvent

Difan Zhang,* Melissa T. Manetsch, Sarah I. Allec, Loukas Kollias, Roger Rousseau, David J. Heldebrant, and Vassiliki-Alexandra Glezakou*

Cite This: https://doi.org/10.1021/acsomega.5c02620

ABSTRACT: Molecular-level insights into reactive separations are crucial for the design of new conversion pathways of carbon dioxide (CO_2). This work explores a postulated pathway that directs CO_2 to undergo inverse-electron-demand Diels–Alder reactions to produce heterocycles using the CO_2 chemically fixed on water-lean solvent molecules. Density functional theory calculations are applied to evaluate the lowest unoccupied molecular orbital (LUMO) energies of three types of reactants (1,3-butadiene, 1,3-cyclohexadiene, and 1,2,4,5-tetrazine) with various functional substituents. These calculations also provide a data set (5.8k data) for developing a machine learning model to efficiently predict LUMO energies. A computational screening of LUMO energies for an additional 47k diene and tetrazine candidates is performed, and a list of candidates with lowered LUMO energies by electron-withdrawing substituents is provided. These candidates are further examined by their reaction energy barriers computed from the interatomic potential or density functional theory. Two major energy barriers are identified, one for the proton transfer within the water-lean solvent and the other for the CO_2 transfer from the solvent molecule to the reactant candidate (diene or tetrazine). The functional substituents have a more significant impact on the second barrier but a very slight one on the first barrier. This exploratory work demonstrates a new possibility for guiding experimental efforts toward the chemical conversion of fixated CO_2 to value-added compounds.

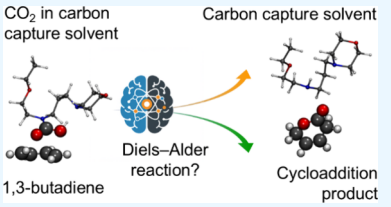

INTRODUCTION

The utilization of common feedstocks is crucial for the efficient production of valuable chemicals. A key obstacle in the chemical conversion of abundant feedstocks such as CO_2 is the kinetic and thermodynamic stability of C=O bonds (dissociation energy ~ 5.5 eV) arising from its highly stable, π-conjugated structure.[1−4] Additional hurdles, such as competing side reactions with more favorable thermodynamics and mass transfer limitations due to the low solubility of CO_2, further hinder its activation and make the process economically uncompetitive.[5,6] Overcoming these challenges often requires extreme reaction conditions, such as high temperatures or pressures, complex catalysts based on metals or metal oxides, or external driving forces such as ultraviolet light.[7−11] Regardless, before we can evaluate possible synthetic routes, a detailed understanding of the thermal chemistry and which products and reaction paths are likely is necessary. While notable advances have been made in CO_2 conversion using metal–organic frameworks[12] and in the photocatalytic conversion of CO_2+H_2O to solar fuels,[13] these technologies are still plagued by the energetic bottleneck of CO_2 activation and its separation from the capture media.

An alternative approach is reactive separations, which, by design, couple separation and conversion processes in the same medium for increased energy efficiency.[14] However, this requires the design of new reaction pathways for CO_2 in diverse environments, including organic solvents and catalyst surfaces, for which molecular-level control is crucial. The chemical conversions of CO_2 are typically restricted to nucleophilic or electrophilic attack, limiting the choice of available reagents to high-energy species (e.g., H^-, epoxides, etc.), which in turn greatly limits the products that can be made.[15] While the water-lean carbon capture solvents are promising media for the thermo-catalytic production of C1 products such as methanol or methane,[14,16] CO_2 utilization approaches will need to move beyond CO_2-neutral products to have any meaningful impact on the efficient utilization of C1 feedstocks.[15,17]

To address this need, we postulate that the unsaturated bonds of "captured" CO_2 could participate in a concerted Diels–Alder (DA) [4 + 2] cycloaddition, which would utilize CO_2 in its entirety without energy-intensive bond breaking as commonly done in other CO_2 utilization approaches. This new reactivity with dienes could significantly contribute to negative emission strategies by widening the field of valuable products that CO_2 could be made into, such as lactones, which are used industrially for flavor and fragrance additives.[18] Lactones are

Received: March 21, 2025
Revised: May 5, 2025
Accepted: May 16, 2025

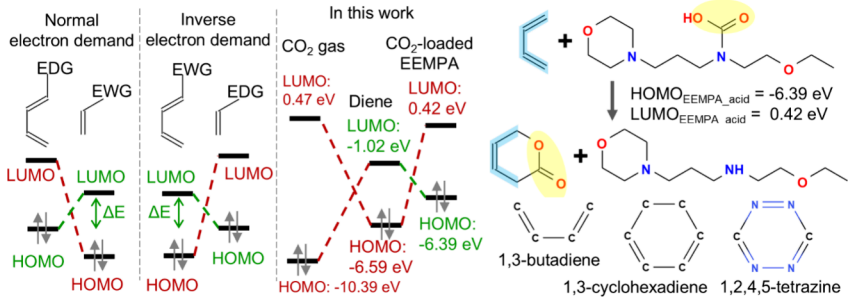

Figure 1. Schematic diagram of normal and inverse-electron-demand DA reactions, where EDG and EWG denote electron-donating and electron-withdrawing groups, respectively. The HOMO and LUMO energies of 1,3-butadiene and CO_2-loaded EEMPA as the dienophile and the proposed reaction are shown on the right side. Three types of molecules are considered: 1,3-butadiene, 1,3-cyclohexadiene, and 1,2,4,5-tetrazine.

also attractive because they are a platform to produce polyesters via ring-opening polymerization,[19] enabling the synthesis of a commodity polymer that can be a sizable and durable CO_2 sink that has not yet been made directly from CO_2.

To our knowledge, there are limited accounts of CO_2 being introduced in cycloaddition reactions.[20] For example, Zhang and Lu[21] and Fernández-Hererra and Merino[22] have demonstrated 1,3 dipolar cycloadditions of CO_2 and hydrazonyl chloride to 1,3,4 oxadiazole-2-(3H)-ones from hydrazonyl chloride. Similarly, Hamlin showed a 1,3 dipolar cycloaddition with CO_2 into nitrilimines, suggesting the mechanism is stepwise, with activation by F^- providing hybridization of CO_2 from *sp* into a more reactive nucleophilic trigonal planar sp^2 anion.[23] Additionally, Lu et al. showed that bis(aminoguanidines) can be used for 1,3 dipolar cycloadditions of "captured" CO_2 with propargylamidine.[24] We note that these pioneering examples of cycloadditions are stepwise cycloadditions that proceed via nucleophilic attack of an activated CO_2-containing anion to a small subset of hydrazonyl chlorides and prop-argylamines, which are distinctly different from a concerted DA [4 + 2] cycloaddition reaction where a common diene would react with captured CO_2 (carbamate) acting as a dienophile.

CO_2 can be fixated as a carbamic acid/carbamate or alkyl carbonic/alkyl carbonate species that are in dynamic equilibrium in solution[25] in organic solvents such as the leading water-lean carbon capture solvent *N*-(2-ethoxyethyl)-3-morpholinopropan-1-amine (EEMPA).[26,27] The anionic alkyl carbonates and carbamates (as dienophiles) favor electron donation, and the captured CO_2 should in principle undergo primarily inverse-demand DA reactions, as illustrated in Figure 1. Here, the frontier molecular orbital theory suggests the greater the overlap between the highest occupied molecular orbital (HOMO) of the electron donor and the lowest unoccupied molecular orbital (LUMO) of the electron acceptor, the lower the reaction barrier.[28−30] Consequently, the HOMO/LUMO energy gaps can indicate the kinetics of DA reactions, although the actual energy barrier is impacted by more complex factors.[31,32] In single-component CO_2 capture solvents (e.g., EEMPA, IPADM,[25] IPATFMM,[25] etc.), the captured CO_2 may carry a negative charge in an sp^2-hybridized state, allowing for the necessary orbital overlap for CO_2 to act as a dienophile. Further, the energies of HOMO/LUMO of dienes can be effectively tuned via functionalization: the HOMO energy is increased by adding electron-rich groups to the electron-donating reactant and the LUMO energy is decreased by adding electron-deficient substituents to the electron-accepting reactant.[33] However, the impact of multiple functional groups at the same time (e.g., the types and locations of more than two functional groups) is still a knowledge gap for CO_2 fixated on EEMPA.

In this work, we aim to understand how functionalization in dienes can be leveraged to lower their LUMO energies to facilitate the inverse demand of DA reactions with fixated CO_2 in EEMPA. A data set of 5839 dienes with their corresponding HOMO/LUMO information was assembled from density functional theory (DFT) calculations. A machine learning (ML) model based on the light gradient boosting machine (LGBM) framework was subsequently developed to screen the LUMO energies of more diene candidates for the inverse-demand DA reactions with EEMPA. Previous studies[34−37] have demonstrated successes in applying ML to understand and predict DA reactions, but they are not aimed at chemically fixated CO_2. To further verify the ML results, our proposed diene candidates based on LUMO screening are examined by transition state calculations using DFT and force fields to evaluate the changes in the reaction energy barriers. Our results serve as a starting point for future experimental investigations. Since DA cycloadditions with molecular or chemically fixated CO_2 in solution (i.e., carbamate) have yet to be thoroughly studied, experimental research in this area will greatly benefit from the design of an optimal coreactant (diene) through computational screening and modeling.[38−40]

METHODS

Since we did not find databases that contain significant numbers of dienes, we constructed our own data set by functionalizing three types of molecules with various substituents. The first type is aliphatic functionalized 1,3-butadiene as shown in the example in Figure 1. To explore the influence of stereochemistry, the second type is nonaliphatic functionalized 1,3-cyclohexadiene. The third type is functionalized 1,2,4,5-tetrazine because it has been reported for inverse-demand DA reactions in many previous studies.[41−44] For substituents, we considered 10 common organic functional groups, including electron-donating groups (EDGs) such as $-N(CH_3)_2$, $-NH_2$, $-SCH_3$, $-OH$, $-OCH_3$, and $-CH_3$ and electron-withdrawing groups (EWGs) such as $-CHO$, $-COOH$, $-SO_2H$, and $-CN$, in our DFT calculations. Then we used the Simplified Molecular-Input Line-Entry System (SMILES) representation of molecules and functional groups to add one, two, or three functional groups to the molecules. The resulting SMILES of the functionalized molecule were converted to three-dimensional coordinates using Open-Babel[45] and RDKit.[46] The generated structures, as well as

https://doi.org/10.1021/acsomega.5c02620
ACS Omega XXXX, XXX, XXX−XXX

EEMPA, were geometrically optimized by DFT calculations to obtain their HOMO and LUMO energies. All DFT calculations were carried out with ORCA[47] using the B3LYP functional,[48,49] Grimme's D3[50] van der Waals corrections, and the def2-TZVP basis set.[51] A preoptimization using the xTB software[52,53] with the GFN2-xTB[53] method was performed to obtain initial structures before DFT optimizations. The xTB-optimized structures were screened to remove unphysical structures due to stereochemistry, and eventually, we obtained 5839 structures containing 48 molecules with one substituent, 692 with two substituents, and 5099 with three substituents. The details of the numbers of molecules in each type are provided in Table S1 in the supporting materials.

The DFT-derived LUMO values of dienes and tetrazines were used to parametrize ML models to evaluate the LUMO values of molecules more efficiently. The RDKit descriptor containing 122 features was generated based on the SMILES strings. The molecular features were further condensed by removing the variables with high correlations (Pearson's correlation coefficients $R > 0.7$). For three-substituted dienes, we used only 40% of the data during the development of the ML model, and the rest 60% of the data was left unseen for prediction evaluation only. As a result, 2779 data are used in the development stage of ML (as training/testing/validation data) and 3060 data are filtered out for future use. The details of the numbers of data in each type of molecule are provided in Table S2. We first split the 2779 data into training, testing, and validation data sets by 60%/20%/20%. To select an appropriate ML algorithm, the data sets were passed into 40 ML algorithms (see Table S3) to parametrize predictive models to estimate the LUMO energies. The algorithm demonstrating the lowest root-mean-square error (RMSE) and the highest correlation coefficient (R^2) value was selected, and a hyperparameter fine-tuning using a 5-fold cross-validation method was performed to finalize the model parameters. All ML training and prediction were performed with the Python package Scikit-learn.[54]

A computational screening of more diene/tetrazine candidates was carried out using our developed ML model. Here, we considered a wider range of functional groups based on previous studies of DA reactions ($-N(CH_3)_2$, $-NHCH_3$, $-NH_2$, $-NHCOCH_3$, $-OH$, $-OCH_3$, $-OC_2H_5$, $-OCOCH_3$, $-CH_3$, $-COH$, $-COCH_3$, $-COOH$, $-COOCH_3$, $-CH_2OH$, $-CONHCH_3$, $-SCH_3$, $-SO_2H$, $-SO_3H$, $-NO_2$, $-CN$)[33,55,56,57,58] up to three substituents on diene/tetrazine. In total, 47560 diene/tetrazine candidates were built and screened. The top ten candidates with the lowest LUMO energies in each type of one-/two-/three-substituted dienes (either butadiene or cyclohexadiene) and one-/two-substituted tetrazines were identified, and their LUMO energies were further verified by DFT calculations again. Then the top five candidates of each type were used to evaluate reaction energy barriers.

The nudged elastic band (NEB) calculations using DFT as implemented in ORCA were first performed for 1,3-butadiene, 1,3-cyclohexadiene, and 1,2,4,5-tetrazine to search for the transition states and compute reaction energy barriers. Since NEB calculations by DFT are extremely time-consuming, the resulting structures of reactants, transition states, and products from these DFT NEB calculations were used to evaluate the accuracy of several MACE force fields reported in the literature[59−61] and the semiempirical GFN2-xTB method.[62] The energies of given structures from DFT were compared to energies computed by these methods, and the method showing the highest accuracy was used to compute the reaction energy landscape after the original dienes and tetrazines were replaced by the top candidates identified in the last step. For transition states, the geometric optimization using the force field was performed by Sella[63] within the framework of ASE. For other states, the geometric optimization was performed using the BFGS optimizer implemented in ASE. All scripts and codes are provided in the GitHub repository https://github.com/zhangdf07/Diels-Alder-CO2.

RESULTS AND DISCUSSION

We first analyzed our 5839 DFT calculations of functionalized 1,3-butadiene, 1,3-cyclohexadiene, and 1,2,4,5-tetrazine molecules. The overall distribution of their LUMO energies is illustrated in Figure 2. Varying the type and position of

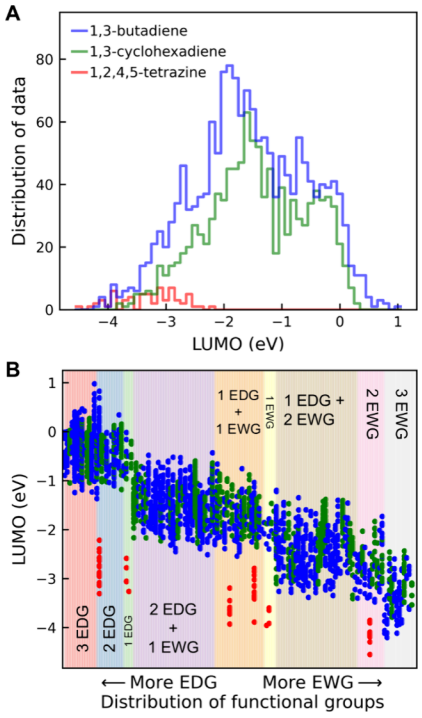

Figure 2. (A) Distribution of LUMO energies in three types of molecules based on substituted 1,3-butadiene, 1,3-cyclohexadiene, and 1,2,4,5-tetrazine. (B) LUMO energy changes with different numbers of EWG and EDG functionalities on various types of molecules. The color scheme of the data points is the same as that of (A). Shaded colors in the background highlight regions with different EWG/EDG ratios.

functional groups significantly impacts the LUMO energies of all three types of molecules, ranging from −4.5 to 1 eV. The tetrazine-based molecules (red, Figure 2A) generally show lower LUMO energies than diene-based molecules (blue and green, Figure 2A). Furthermore, the LUMO energy change with different numbers and types of EWG/EDG groups is highlighted in Figure 2B. It is not surprising that for all three types of molecules increasing the numbers of EWG groups gradually lowers the LUMO energies. For the same numbers of EWG/EDG groups, tetrazine-based molecules (red) show about 1−2 eV lower LUMO energies than diene-based molecules (blue and green). The results of substituted 1,3-butadiene (blue) and substituted 1,3-cyclohexadiene (green)

https://doi.org/10.1021/acsomega.5c02620
ACS Omega XXXX, XXX, XXX−XXX

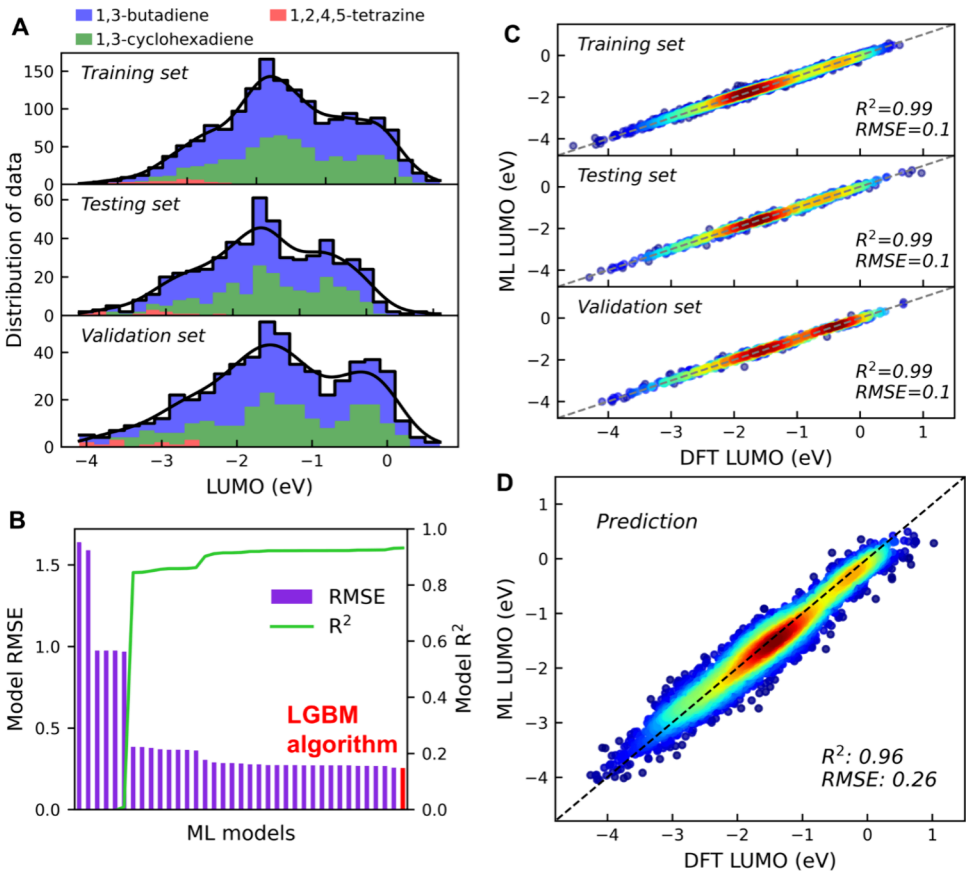

Figure 3. (A) Stack bar graph for the data set, which splits DFT data into training, testing, and validation for ML algorithm selection. The black solid smooth line shows the overall trend of the data distribution. (B) Average RMSE and R^2 of the testing and validation data sets using 40 ML algorithms. The algorithm with the lowest RMSE and the highest R^2 is highlighted. (C) ML-predicted LUMO energies using the LGBM method after a hyperparameter tuning with 5-fold cross-validation. Data points are colored by their local distribution density, with red indicating dense data points and blue indicating loose data points. (D) LUMO prediction of dienes outside the data used in the ML parametrization stage. Data points are colored by their local distribution density.

strongly overlap across different functional groups, suggesting a minor impact of stereochemistry on their LUMO energies.

To explore even more substituent groups in dienes or tetrazines and avoid the computational cost of tens of thousands of DFT calculations, we used our DFT data to develop an ML model that can quickly evaluate the LUMO energies of a functionalized 1,3-butadiene, 1,3-cyclohexadiene, or 1,2,4,5-tetrazine. As stated in the Methods section, here, we only used 2779 data in the development stage of ML, while the remaining 3060 data were saved as unseen data to examine the predictive accuracy of our ML model. As shown in Figure 3A, the data in each type of dienes and tetrazines are split into training, testing, and validation data sets to reduce any bias during evaluation. Their combined training set was used to parametrize 40 ML models of different algorithms without any hyperparameter tuning. The combined testing and validation sets were used to examine the predictive power of the parametrized ML models to avoid overfitting. The average performance on the testing and validation sets is demonstrated in Figure 3B, and the full names and numerical values of these models are provided in Table S3. We identified several ML algorithms with similarly high accuracy, such as gradient boosting, hist gradient boosting, and LGBM. Since LGBM showed the lowest time cost and memory usage as well as the lowest RMSE and highest R^2, it was selected to be further refined.

A hyperparameter tuning was then performed on the LGBM model using 5-fold cross-validation to optimize parameters including the maximum tree leaves, the maximum tree depth, boosting learning rate, the number of boosted trees, sample numbers for bins, and subsample ratios of trees. The optimized model and parameters are provided in our shared GitHub repository. The performance of the refined model is provided in Figure 3C. Both RMSE and R^2 metrics were further improved after hyperparameter tuning. The specific breakdown performance of each type of molecule (butadiene, cyclohexadiene, and tetrazine) is provided in Figure S1. All data sets and molecule types show similar accuracy due to the application of cross-validation. The developed LGBM model is also not biased toward a particular molecule type regardless of the number of data points (Figure S1d). Moreover, to further examine the predictive power of the refined LGBM model, we used the model to compute the LUMO energies of the 3060 unseen molecules we saved at the beginning (outside the data used in ML parametrization) as shown in Figure 3D. The 3060 ML-computed LUMO energies show comparable accuracy to the 2779 data sets used in the parametrization stage. Therefore, we believe our refined LGBM model is adequately precise to evaluate the LUMO energies of functionalized butadiene, cyclohexadiene, and tetrazine, and it is suitable for conducting a computational screening of additional molecules.

https://doi.org/10.1021/acsomega.5c02620
ACS Omega XXXX, XXX, XXX−XXX

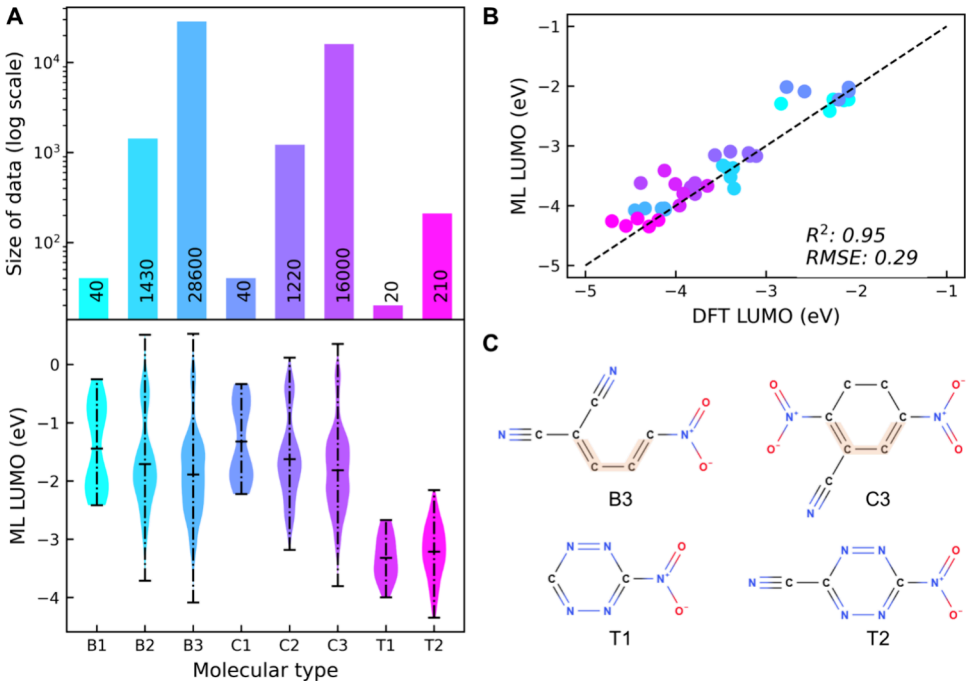

Figure 4. (A) Numbers of functionalized dienes and tetrazines considered in the computational screening by ML (top) and the distribution of their ML-predicted LUMO energies (bottom). Numbers in the top bar graph indicate the numerical values of the data sizes. For labels on the horizontal axis, B1, B2, and B3 indicate the 1,3-butadiene with one-/two-/three-substituent groups, respectively. C1, C2, and C3 indicate the 1,3-cyclohexadiene with one-/two-/three-substituent groups, respectively. T1 and T2 indicate the 1,2,4,5-tetrazine with one-/two-substituent groups, respectively. (B) Comparison of LUMO energies between ML and DFT for the selected candidates. The color scheme of data points is the same as plot (A). (C) Examples of selected diene (B3 and C3) and tetrazine (T1 and T2) molecules. Shaded colors highlight the diene segment of the molecule.

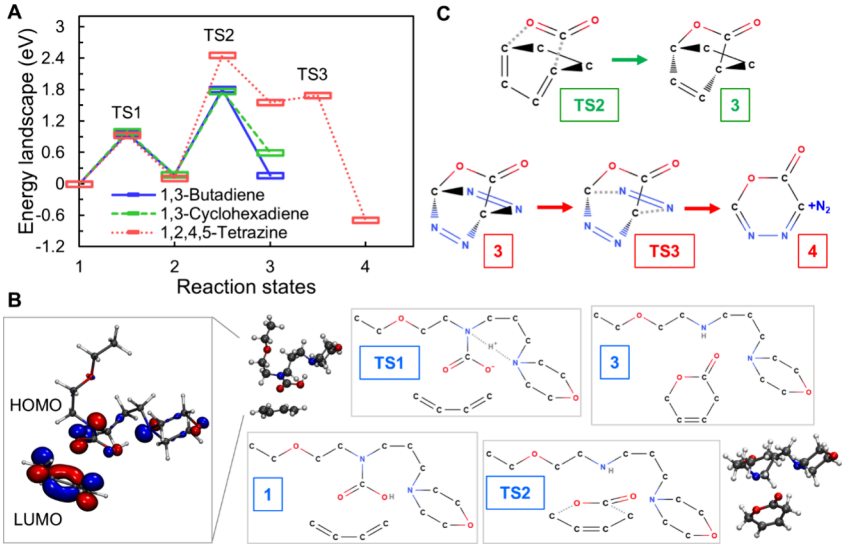

Figure 5. (A) Reaction energy landscapes for 1,3-butadiene, 1,3-cyclohexadiene, and 1,2,4,5-tetrazine, computed by NEB calculations using DFT. (B) Schematic snapshots of structures observed in the pathway of 1,3-butadiene. Molecular snapshots on the left and right sides highlight the initial reactant complex and final product complex geometries, respectively. C, H, O, and N are shown in black, white, red, and blue colors, respectively. The diene LUMO and dienophile HOMO orbitals are highlighted on the left side. (C) Change of the second transition state for 1,3-cyclohexadiene (top, green arrow) and the third reaction step for 1,2,4,5-tetrazine (bottom, red arrow).

We considered a wider range of substituent groups in the screening by the ML method as discussed in the Methods section. In particular, 30070 functionalized 1,3-butadiene (labeled as B1, B2, or B3 to indicate one-/two-/three-substituted butadiene), 17260 functionalized 1,3-cyclohexadiene (labeled as C1, C2, or C3 to indicate one-/two-/three-substituted cyclohexadiene), and 230 functionalized 1,2,4,5-tetrazine (labeled as T1 or T2 to indicate one-/two-substituted tetrazine) molecules are included in our screening. The distribution of these molecules and the corresponding ML-predicted LUMO energies are illustrated in Figure 4A. For each type of molecule (B, C, or T marked in Figure 4A), the LUMO energies span a wider range as the number of substituent groups increases. Overall, the lowest possible

https://doi.org/10.1021/acsomega.5c02620
ACS Omega XXXX, XXX, XXX−XXX

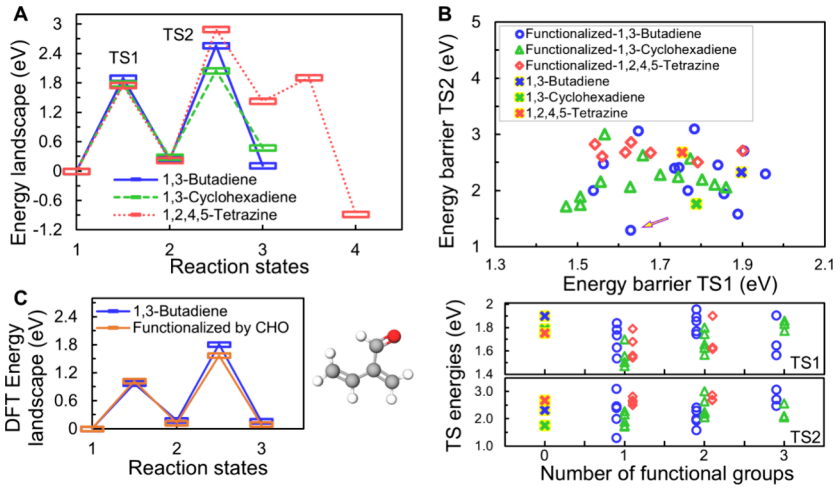

Figure 6. (A) Reaction energy landscapes for 1,3-butadiene, 1,3-cyclohexadiene, and 1,2,4,5-tetrazine, computed by the MACE force field. (B) Energy barriers of the two transition states along the reaction path for ML-selected candidates (top row) and the influence of the number of functional groups on these barriers (bottom row). The molecule pointed out by the arrow is used in the verification of DFT calculations. (C) Comparing the reaction energy landscape of 1,3-butadiene and aldehyde-functionalized 1,3-butadiene, computed by NEB calculations using DFT. The molecular snapshot illustrates the structure of the functionalized molecule, where carbon, hydrogen, and oxygen are in gray, white, and red colors, respectively.

LUMO energies decrease with an increasing number of substituent groups. The three-substituted 1,3-butadiene and 1,3-cyclohexadiene, as well as the one-/two-substituted tetrazine, generally provide lower LUMO energies than the others. We then selected the candidates in each type with the lowest LUMO energies and recomputed their LUMO energies at the DFT level to support the fidelity of ML predictions and to further narrow down the list of candidates. Figure 4B highlights the five candidates in each category with the lowest LUMO energies. Again, the ML-predicted LUMO energies agree well with the DFT-computed values. The full list of these candidates is provided in Figure S2, and four examples of these candidates are visualized in Figure 4C. Functionalization by a strong EWG is important for achieving lower LUMO energies in all cases. For 1,3-butadiene and 1,3-cyclohexadiene, we find that the functionalization of positions 1 and 4 is often necessary. For 1,2,4,5-tetrazine, two substituent groups often lower LUMO more than one substituent group, but their difference is less significant than the dienes' case. The typical HOMO/LUMO energy gaps for inverse-demand DA can be as low as 1.5 eV based on previous reports,[64−69] which is close to our candidates (gaps around 1.4−2.2 eV).

Up to this point, we have narrowed down the candidates to a list of 40 molecules including three categories (functionalized 1,3-butadiene, functionalized 1,3-cyclohexadiene, and functionalized 1,2,4,5-tetrazine), each of which contains one-, two-, or three-substituent groups in the molecules. The lowest LUMO energies are mostly found in bisubstituted tetrazine and trisubstituted butadiene and cyclohexadiene. On the other hand, the HOMO/LUMO gap alone does not capture the full complexity of the reaction energy landscape including the reaction energy barrier of the transition state. Therefore, we further examine these candidates by evaluating their reaction transition states and energy barriers along the pathway via DA cycloaddition reactions.

We performed NEB calculations for 1,3-butadiene, 1,3-cyclohexadiene, and 1,2,4,5-tetrazine at the DFT level of theory. The identified DA reaction pathways and transition states are listed in Figure 5. The 1,3-butadiene and 1,3-cyclohexadiene show pathways similar to those illustrated in Figure 5A,B, where the reaction occurs in a two-step pattern. The first step is initiated by the proton transfer (from state 1 to state 2) within the CO_2-loaded EEMPA molecule, which has a transition state (TS1) energy barrier of 0.98 ± 0.01 eV. The second step is the binding of CO_2 to the diene molecule (from state 2 to state 3) with a transition state (TS2) energy barrier of 1.61 ± 0.02 eV. Compared to our previous calculation on the DA reaction energy barrier of CO_2 gas molecules with 1,3-butadiene (2.7 eV), utilizing EEMPA-captured CO_2 reduces the energy barrier by 1.1 eV. The final product of 1,3-cyclohexadiene (green) shows higher energy than that of 1,3-butadiene (blue) because more stereometric distortion is introduced, as shown in Figure 5C. A similar DA reactivity with out-of-plane distortion has also been quantified in a previous work.[65] Nonetheless, the LUMO of the diene and the HOMO of the dienophile remain accessible for the DA reaction to proceed in all cases, despite the presence of steric repulsion between the two molecules. This suggests that fundamental orbital interactions required for cycloaddition are at play. However, it is important to recognize that while HOMO/LUMO energy levels can serve as an initial indicator of the likelihood of the reaction, they do not fully account for the complexity of molecular interactions in these reactive systems. Additional factors, including electrostatic interactions, polarization effects, dispersion forces, and steric hindrance, can substantially alter the spatial arrangement of atoms in the transition states. These effects, in turn, play a critical role in modulating the reaction energy barriers and, ultimately, the selectivity of the DA process. We also note that reasonable reaction rates may require elevated pressures or mildly elevated reaction temperatures or the use of a catalyst. For 1,2,4,5-tetrazine, the first two steps follow the same mechanism as dienes, but the reaction energy barrier of the second step (TS2, 2.35 eV) is higher than that of dienes due to the stabilization of the conjugated structure in tetrazine. In addition, we also observed a third step (from state 3 to state 4) with a low energy barrier (TS3, 0.13 eV), resulting in the retro-DA reaction that releases a N_2 gas molecule, as illustrated in Figure

https://doi.org/10.1021/acsomega.5c02620
ACS Omega XXXX, XXX, XXX−XXX

5C. Such retro-DA reactions have been observed in previous studies of DA reactions using tetrazine.[43,44]

To mitigate the computational cost of NEB calculations at the DFT level of theory, we explored several computationally cheaper methods such as semiempirical GFN2-xTB[62] and pretrained MACE force fields.[59−61] We used the structures identified in the DFT/NEB calculations and compared their energies between DFT and other methods, as shown in Figure S3. Overall, only the MACE-ANI-CC force field[61] demonstrates consistently reliable performance across the three types of molecules. The energies of stable states (i.e., nontransition states) computed by MACE-ANI-CC correlate linearly well with DFT, but the transition state energies are slightly overestimated by MACE-ANI-CC. This is not too surprising because MACE-ANI-CC was mostly parametrized by stable-state conformers and involved fewer transition state structures. Nonetheless, we believe that MACE-ANI-CC is still the proper option among the methods we considered here. In addition, since only C, H, O, and N elements are considered in the MACE-ANI-CC force field, molecules containing S elements are neglected in energy landscape evaluation by the force field.

We then computed the energy landscapes of the original three molecules (1,3-butadiene, 1,3-cyclohexadiene, and 1,2,4,5-tetrazine) used in Figure 5A and the new candidate molecules from ML screening using the MACE-ANI-CC force field. The results of the original three molecules are illustrated in Figure 6A. In general, the two-/three-step patterns in DFT/NEB results were reproduced, and the trends of reactants, intermediates, and products were consistent with DFT results. However, as discussed in the last paragraph, the force field overestimated most transition state energies, leading to estimated energy barriers of 1.81 ± 0.06 eV (TS1), 2.25 ± 0.47 eV (TS2), and 0.47 eV (TS3 for tetrazine). Compared to DFT/NEB results, these barriers were overestimated by 78%−95% for TS1, 10−40% for TS2, and 2.6 times for TS3.

The TS1 and TS2 energy barriers of the new candidate molecules from ML screening are highlighted in Figure 6B. The addition of functional substituent groups could influence both energy barriers for all three types of molecules. The effects on the TS1 and TS2 energy barriers are independent. For the TS1 barrier, the magnitude of impact is less significant for all molecules, and the TS1 energy barriers were only changed within the 0.5 eV range (from 1.47 to 1.96 eV). For the TS2 barrier, the functionalized butadiene and cyclohexadiene molecules could vary more significantly within the 1.8 eV range (from 1.3 to 3.1 eV), but the functionalized tetrazines only demonstrated changes within a limited range of 0.4 eV (from 2.5 to 2.86 eV). Moreover, unlike the computed LUMO energies, the energy barriers do not follow a generally decreasing trend with an increasing number of added EWG groups. This agrees with our understanding that LUMO energy cannot fully describe the change of transition state energy barriers, although computational screening of LUMO energy is much easier. The TS2 barrier demonstrates more adjustable behavior by the organic functionalization of diene/tetrazine molecules, and a single substituent group seems to be a more effective way to lower the overall energy barriers.

Since TS2 is more tunable than TS1 by functionalization, we selected a candidate that drastically lowered the TS2 barrier and verified its reaction pathway by the more accurate NEB calculations at the DFT level. As shown in Figure 6C, although there is a quantitative discrepancy, the DFT/NEB calculation qualitatively validates the MACE force field's suggestion that the proper functionalized diene reduces the reaction energy barrier of TS2 (from 1.63 to 1.45 eV) but has a limited impact on the TS1 barrier. To further reduce these kinetic barriers along the reaction pathway, additional methods other than functionalization will no doubt be needed, such as catalysts, but this is beyond the scope of this work.

CONCLUSIONS

In this work, we employed first-principles DFT calculations and ML to explore the conversion pathway of CO_2 into heterocycles via the inverse-electron-demand DA reaction between dienes/tetrazines and EEMP-fixated C1 feedstock (here, CO_2 acted as the dienophile). We assembled a DFT-based data set of LUMO energies, allowing for the development of an ML model to perform a rapid screening of LUMO energies for additional diene/tetrazine molecules. Increasing the number of electron-withdrawing substituents reduces the LUMO energies of diene and tetrazine molecules, making them more electron-deficient to enable the captured CO_2 to act as the electron donor. The trisubstituted 1,3-butadiene and 1,3-cyclohexadiene and the single-/bisubstituted tetrazine molecules generally demonstrated lower LUMO energies than the others. The reaction energy barriers of the selected candidates from ML screening were further examined by the force field and DFT methods. A two-step reaction pathway was identified, where the first step is initiated with a proton transfer within EEMPA. In a second step, the C1 reactant decouples from the activating agent (EEMPA) and transfers to diene/tetrazine. The functionalization of diene/tetrazine shows a significant impact on the energy barrier of the second step and only limited influence on the first step. We envision that the predictions presented here can serve as input to experimental works to synthesize new candidates and encourage subsequent experimental investigations of reaction conditions that can mitigate side reactions and expand C1-feedstock conversion into valuable target chemicals. A more focused analysis involving the free energy landscape in the reaction medium using molecular dynamics or enhanced sampling methods is also warranted to fully reveal the underlying mechanisms and kinetics for the selected candidates.

ASSOCIATED CONTENT

Data Availability Statement

All of the scripts needed to reproduce results and figures in the manuscript and Supporting Information are available on GitHub https://github.com/zhangdf07/Diels-Alder-CO2. Additional detail is provided in the description section of the GitHub repository.

Supporting Information

The Supporting Information is available free of charge at https://pubs.acs.org/doi/10.1021/acsomega.5c02620.

Detailed information on data distribution of different types of dienes and tetrazines used in the DFT and ML calculations, numeric values of various ML algorithms, predicted LUMO energies by ML in specific types and their overall performance, list of selected diene and tetrazine candidates from ML screening, and the benchmark of force field and semiempirical methods compared to DFT energy (PDF)

https://doi.org/10.1021/acsomega.5c02620
ACS Omega XXXX, XXX, XXX−XXX

AUTHOR INFORMATION

Corresponding Authors

Difan Zhang − *Physical and Computational Sciences Directorate, Pacific Northwest National Laboratory, Richland, Washington 99352, United States;* Present Address: Chemical Sciences Division, Physical Sciences Directory, Oak Ridge National Laboratory, Oak Ridge, Tennessee 37831, United States; orcid.org/0000-0001-7530-2378; Email: difan.zhang@pnnl.gov

Vassiliki-Alexandra Glezakou − *Chemical Sciences Division, Physical Sciences Directory, Oak Ridge National Laboratory, Oak Ridge, Tennessee 37831, United States;* orcid.org/0000-0001-6028-7021; Email: glezakouva@ornl.gov

Authors

Melissa T. Manetsch − *Physical and Computational Sciences Directorate, Pacific Northwest National Laboratory, Richland, Washington 99352, United States;* Present Address: Department of Chemical and Biomolecular Engineering, Massachusetts Institute of Technology, Cambridge, Massachusetts 02139, United States.; orcid.org/0000-0003-3721-6131

Sarah I. Allec − *Physical and Computational Sciences Directorate, Pacific Northwest National Laboratory, Richland, Washington 99352, United States;* orcid.org/0000-0002-1101-3160

Loukas Kollias − *Physical and Computational Sciences Directorate, Pacific Northwest National Laboratory, Richland, Washington 99352, United States;* Present Address: School of Chemical Engineering, National Technical University of Athens, Zografou 15780, Greece.; orcid.org/0000-0002-2114-1238

Roger Rousseau − *Chemical Sciences Division, Physical Sciences Directory, Oak Ridge National Laboratory, Oak Ridge, Tennessee 37831, United States;* orcid.org/0000-0003-1947-0478

David J. Heldebrant − *Physical and Computational Sciences Directorate and Energy Processes and Materials, Energy and Environment Directorate, Pacific Northwest National Laboratory, Richland, Washington 99352, United States; Chemical Engineering and Bioengineering, Washington State University, Pullman, Washington 99164, United States;* orcid.org/0000-0002-5529-526X

Complete contact information is available at: https://pubs.acs.org/10.1021/acsomega.5c02620

Notes

The authors declare no competing financial interest.

ACKNOWLEDGMENTS

The authors acknowledge the U.S. Department of Energy (DOE), Office of Science, Basic Energy Sciences, Chemical Sciences, Geosciences, and Biosciences Division, Harnessing Confinement Effects, Stimuli, and Reactive Intermediates in Separations, FWP 81462. M.T.M. acknowledges support from the U.S. DOE, Office of Science, Office of Workforce Development for Teachers and Scientists (WDTS) under the Science Undergraduate Laboratory Internship (SULI) program. V.-A.G. acknowledges partial support from ORNL's LDRD program. Computational resources were provided by the National Energy Research Scientific Computing Center (NERSC), a Department of Energy Office of Science User Facility, using NERSC award BES ERCAP0031452.

REFERENCES

(1) Dutcher, B.; Fan, M.; Russell, A. G. Amine-Based CO2 Capture Technology Development from the Beginning of 2013—A Review. *ACS Appl. Mater. Interfaces* **2015**, *7* (4), 2137−2148.

(2) Figueroa, J. D.; Fout, T.; Plasynski, S.; McIlvried, H.; Srivastava, R. D. Advances in CO2 capture technology—The U.S. Department of Energy's Carbon Sequestration Program. *International Journal of Greenhouse Gas Control* **2008**, *2* (1), 9−20.

(3) Leung, D. Y. C.; Caramanna, G.; Maroto-Valer, M. M. An overview of current status of carbon dioxide capture and storage technologies. *Renewable and Sustainable Energy Reviews* **2014**, *39*, 426−443.

(4) Wang, M.; Lawal, A.; Stephenson, P.; Sidders, J.; Ramshaw, C. Post-combustion CO2 capture with chemical absorption: A state-of-the-art review. *Chem. Eng. Res. Des.* **2011**, *89* (9), 1609−1624.

(5) Aresta, M.; Dibenedetto, A.; Angelini, A. Catalysis for the Valorization of Exhaust Carbon: from CO2 to Chemicals, Materials, and Fuels. Technological Use of CO2. *Chem. Rev.* **2014**, *114* (3), 1709−1742.

(6) Álvarez, A.; Borges, M.; Corral-Pérez, J. J.; Olcina, J. G.; Hu, L.; Cornu, D.; Huang, R.; Stoian, D.; Urakawa, A. CO2 Activation over Catalytic Surfaces. *ChemPhysChem* **2017**, *18* (22), 3135−3141.

(7) Ma, J.; Sun, N.; Zhang, X.; Zhao, N.; Xiao, F.; Wei, W.; Sun, Y. A short review of catalysis for CO2 conversion. *Catal. Today* **2009**, *148* (3), 221−231.

(8) Etim, U. J.; Zhang, C. C.; Zhong, Z. Y. Impacts of the Catalyst Structures on CO2 Activation on Catalyst Surfaces. *Nanomaterials* **2021**, *11* (12), 3265.

(9) Yin, X.; Moss, J. R. Recent developments in the activation of carbon dioxide by metal complexes. *Coord. Chem. Rev.* **1999**, *181* (1), 27−59.

(10) Erno, Z.; Asadirad, A. M.; Lemieux, V.; Branda, N. R. Using light and a molecular switch to 'lock' and 'unlock' the Diels-Alder reaction. *Organic & Biomolecular Chemistry* **2012**, *10* (14), 2787−2792.

(11) Lin, S.; Ischay, M. A.; Fry, C. G.; Yoon, T. P. Radical Cation Diels-Alder Cycloadditions by Visible Light Photocatalysis. *J. Am. Chem. Soc.* **2011**, *133* (48), 19350−19353.

(12) Trickett, C. A.; Helal, A.; Al-Maythalony, B. A.; Yamani, Z. H.; Cordova, K. E.; Yaghi, O. M. The chemistry of metal-organic frameworks for CO2 capture, regeneration and conversion. *Nature Reviews Materials* **2017**, *2* (8), 1−16.

(13) Li, X.; Yu, J.; Jaroniec, M.; Chen, X. Cocatalysts for selective photoreduction of CO 2 into solar fuels. *Chem. Rev.* **2019**, *119* (6), 3962−4179.

(14) Kothandaraman, J.; Lopez, J. S.; Jiang, Y.; Walter, E. D.; Burton, S. D.; Dagle, R. A.; Heldebrant, D. J. Integrated Capture and Conversion of CO2 to Methane Using a Water-lean, Post-Combustion CO2 Capture Solvent. *ChemSusChem* **2021**, *14* (21), 4812−4819.

(15) Heldebrant, D. J.; Kothandaraman, J.; Dowell, N. M.; Brickett, L. Next steps for solvent-based CO2 capture; integration of capture, conversion, and mineralisation. *Chemical Science* **2022**, *13* (22), 6445−6456.

(16) Kothandaraman, J.; Dagle, R. A.; Dagle, V. L.; Davidson, S. D.; Walter, E. D.; Burton, S. D.; Hoyt, D. W.; Heldebrant, D. J. Condensed-phase low temperature heterogeneous hydrogenation of CO2 to methanol. *Catal. Sci. Technol.* **2018**, *8* (19), 5098−5103.

(17) Appel, A. M.; Bercaw, J. E.; Bocarsly, A. B.; Dobbek, H.; DuBois, D. L.; Dupuis, M.; Ferry, J. G.; Fujita, E.; Hille, R.; Kenis, P. J. A.; et al. Frontiers, Opportunities, and Challenges in Biochemical and Chemical Catalysis of CO2 Fixation. *Chem. Rev.* **2013**, *113* (8), 6621−6658.

(18) Paulino, B. N.; Sales, A.; Felipe, L.; Pastore, G. M.; Molina, G.; Bicas, J. L. Recent advances in the microbial and enzymatic

production of aroma compounds. *Current Opinion in Food Science* **2021**, *37*, 98−106.
(19) Albertsson, A.-C.; Varma, I. K. Recent Developments in Ring Opening Polymerization of Lactones for Biomedical Applications. *Biomacromolecules* **2003**, *4* (6), 1466−1486.
(20) McLeod, D.; Thøgersen, M. K.; Jessen, N. I.; Jørgensen, K. A.; Jamieson, C. S.; Xue, X.-S.; Houk, K. N.; Liu, F.; Hoffmann, R. Expanding the Frontiers of Higher-Order Cycloadditions. *Acc. Chem. Res.* **2019**, *52* (12), 3488−3501.
(21) Guo, C. X.; Zhang, W. Z.; Zhang, N.; Lu, X. B. 1,3-Dipolar Cycloaddition of Nitrile Imine with Carbon Dioxide: Access to 1,3,4-Oxadiazole-2(3H)-ones1,3-Dipolar Cycloaddition of Nitrile Imine with Carbon Dioxide: Access to 1,3,4-Oxadiazole-2(3H)-ones. *J. Org. Chem.* **2017**, *82* (14), 7637−7642.
(22) Murillo, F.; Barroso, J.; de los Santos, M. G.; Avila, G.; Pan, S.; Fernandez-Herrera, M. A.; Merino, G. Revisiting the Formation Mechanism of 1,3,4-Oxadiazole-2(3H)-ones from Hydrazonyl Chloride and Carbon Dioxide. *J. Org. Chem.* **2018**, *83* (21), 13045−13050.
(23) Svatunek, D.; Hansen, T.; Houk, K. N.; Hamlin, T. A. How the Lewis Base F- Catalyzes the 1,3-Dipolar Cycloaddition between Carbon Dioxide and Nitrilimines. *J. Org. Chem.* **2021**, *86* (5), 4320−4325.
(24) Zhou, H.; Chen, W.; Liu, J. H.; Zhang, W. Z.; Lu, X. B. Highly effective capture and subsequent catalytic transformation of low-concentration CO2 by superbasic guanidines. *Green Chem.* **2020**, *22* (22), 7832−7838.
(25) Cantu, D. C.; Lee, J.; Lee, M. S.; Heldebrant, D. J.; Koech, P. K.; Freeman, C. J.; Rousseau, R.; Glezakou, V. A. Dynamic Acid/Base Equilibrium in Single Component Switchable Ionic Liquids and Consequences on Viscosity. *J. Phys. Chem. Lett.* **2016**, *7* (9), 1646−1652.
(26) Zheng, R. F.; Barpaga, D.; Mathias, P. M.; Malhotra, D.; Koech, P. K.; Jiang, Y.; Bhakta, M.; Lail, M.; Rayer, A. V.; Whyatt, G. A.; et al. A single-component water-lean post-combustion CO2 capture solvent with exceptionally low operational heat and total costs of capture − comprehensive experimental and theoretical evaluation. *Energy Environ. Sci.* **2020**, *13* (11), 4106−4113.
(27) Cantu, D. C.; Malhotra, D.; Nguyen, M.-T.; Koech, P. K.; Zhang, D.; Glezakou, V.-A.; Rousseau, R.; Page, J.; Zheng, R.; Perry, R. J.; et al. Molecular-Level Overhaul of γ-Aminopropyl Amino-silicone/Triethylene Glycol Post-Combustion CO2-Capture Solvents. *ChemSusChem* **2020**, *13* (13), 3429−3438.
(28) Nandi, S.; Monesi, A.; Drgan, V.; Merzel, F.; Novič, M. Quantitative structure-activation barrier relationship modeling for Diels-Alder ligations utilizing quantum chemical structural descriptors. *Chemistry Central Journal* **2013**, *7* (1), 171.
(29) Parr, R. G.; Yang, W. Density functional approach to the frontier-electron theory of chemical reactivity. *J. Am. Chem. Soc.* **1984**, *106* (14), 4049−4050.
(30) Yu, J.; Su, N. Q.; Yang, W. Describing Chemical Reactivity with Frontier Molecular Orbitalets. *JACS Au* **2022**, *2* (6), 1383−1394.
(31) Sauer, J.; Sustmann, R. Mechanistic Aspects of Diels-Alder Reactions: A Critical Survey. *Angewandte Chemie International Edition in English* **1980**, *19* (10), 779−807.
(32) Martin, J. G.; Hill, R. K. Stereochemistry of the Diels-Alder Reaction. *Chem. Rev.* **1961**, *61* (6), 537−562.
(33) Kahn, S. D.; Pau, C. F.; Overman, L. E.; Hehre, W. J. Modeling chemical reactivity. 1. Regioselectivity of Diels-Alder cycloadditions of electron-rich dienes with electron-deficient dienophiles. *J. Am. Chem. Soc.* **1986**, *108* (23), 7381−7396.
(34) Vargas, S.; Hennefarth, M. R.; Liu, Z.; Alexandrova, A. N. Machine Learning to Predict Diels-Alder Reaction Barriers from the Reactant State Electron Density. *J. Chem. Theory Comput.* **2021**, *17* (10), 6203−6213.
(35) Keto, A.; Guo, T.; Underdue, M.; Stuyver, T.; Coley, C. W.; Zhang, X.; Krenske, E. H.; Wiest, O. Data-Efficient, Chemistry-Aware Machine Learning Predictions of Diels-Alder Reaction Outcomes. *J. Am. Chem. Soc.* **2024**, *146* (23), 16052−16061.
(36) Young, T. A.; Johnston-Wood, T.; Zhang, H.; Duarte, F. Reaction dynamics of Diels-Alder reactions from machine learned potentials. *Phys. Chem. Chem. Phys.* **2022**, *24* (35), 20820−20827.
(37) Beker, W.; Gajewska, E. P.; Badowski, T.; Grzybowski, B. A. Prediction of Major Regio-, Site-, and Diastereoisomers in Diels-Alder Reactions by Using Machine-Learning: The Importance of Physically Meaningful Descriptors. *Angew. Chem., Int. Ed.* **2019**, *58* (14), 4515−4519.
(38) Yang, Y.; Zhang, X.; Zhong, L.-P.; Lan, J.; Li, X.; Li, C.-C.; Chung, L. W. Unusual KIE and dynamics effects in the Fe-catalyzed hetero-Diels-Alder reaction of unactivated aldehydes and dienes. *Nat. Commun.* **2020**, *11* (1), 1850.
(39) Vermeeren, P.; Hamlin, T. A.; Fernández, I.; Bickelhaupt, F. M. How Lewis Acids Catalyze Diels-Alder Reactions. *Angew. Chem., Int. Ed.* **2020**, *59* (15), 6201−6206.
(40) Blyth, M. T.; Noble, B. B.; Russell, I. C.; Coote, M. L. Oriented Internal Electrostatic Fields Cooperatively Promote Ground- and Excited-State Reactivity: A Case Study in Photochemical CO2 Capture. *J. Am. Chem. Soc.* **2020**, *142* (1), 606−613.
(41) Hamasaki, A.; Ducray, R.; Boger, D. L. Two Novel 1,2,4,5-Tetrazines that Participate in Inverse Electron Demand Diels−Alder Reactions with an Unexpected Regioselectivity. *Journal of Organic Chemistry* **2006**, *71* (1), 185−193.
(42) Boger, D. L.; Schaum, R. P.; Garbaccio, R. M. Regioselective Inverse Electron Demand Diels−Alder Reactions of N-Acyl 6-Amino-3-(methylthio)-1,2,4,5-tetrazines. *Journal of Organic Chemistry* **1998**, *63* (18), 6329−6337.
(43) Houszka, N.; Mikula, H.; Svatunek, D. Substituent Effects in Bioorthogonal Diels-Alder Reactions of 1,2,4,5-Tetrazines. Chemistry − A. *European Journal* **2023**, *29* (29), No. e202300345.
(44) Sauer, J.; Heldmann, D. K.; Hetzenegger, J.; Krauthan, J.; Sichert, H.; Schuster, J. 1,2,4,5-Tetrazine: Synthesis and Reactivity in [4 + 2] Cycloadditions. *Eur. J. Org. Chem.* **1998**, *1998* (12), 2885−2896.
(45) O'Boyle, N. M.; Banck, M.; James, C. A.; Morley, C.; Vandermeersch, T.; Hutchison, G. R. Open Babel: An open chemical toolbox. *Journal of Cheminformatics* **2011**, *3* (1), 33.
(46) Landrum, G., RDKIT: Cheminformatics and machine-learning software in C++ and Python, For the originating project, see https://www.rdkit.org/, 2020.
(47) Neese, F.; Wennmohs, F.; Becker, U.; Riplinger, C. The ORCA quantum chemistry program package. *J. Chem. Phys.* **2020**, *152* (22), 224108.
(48) Becke, A. D. Density-functional exchange-energy approximation with correct asymptotic behavior. *Phys. Rev. A* **1988**, *38* (6), 3098−3100.
(49) Lee, C.; Yang, W.; Parr, R. G. Development of the Colle-Salvetti correlation-energy formula into a functional of the electron density. *Phys. Rev. B* **1988**, *37* (2), 785−789.
(50) Grimme, S.; Antony, J.; Ehrlich, S.; Krieg, H. A consistent and accurate ab initio parametrization of density functional dispersion correction (DFT-D) for the 94 elements H-Pu. *J. Chem. Phys.* **2010**, *132* (15), 154104.
(51) Weigend, F.; Ahlrichs, R. Balanced basis sets of split valence, triple zeta valence and quadruple zeta valence quality for H to Rn: Design and assessment of accuracy. *Phys. Chem. Chem. Phys.* **2005**, *7* (18), 3297−3305.
(52) Bannwarth, C.; Caldeweyher, E.; Ehlert, S.; Hansen, A.; Pracht, P.; Seibert, J.; Spicher, S.; Grimme, S. Extended tight-binding quantum chemistry methods. *WIREs Computational Molecular Science* **2021**, *11* (2), No. e1493.
(53) Grimme, S.; Bannwarth, C.; Shushkov, P. A Robust and Accurate Tight-Binding Quantum Chemical Method for Structures, Vibrational Frequencies, and Noncovalent Interactions of Large Molecular Systems Parametrized for All spd-Block Elements (Z = 1−86). *J. Chem. Theory Comput.* **2017**, *13* (5), 1989−2009.
(54) Pedregosa, F.; Varoquaux, G.; Gramfort, A.; Michel, V.; Thirion, B.; Grisel, O.; Blondel, M.; Prettenhofer, P.; Weiss, R.;

https://doi.org/10.1021/acsomega.5c02620
ACS Omega XXXX, XXX, XXX−XXX

Dubourg, V.; et al. Scikit-learn: Machine Learning in Python. *J. Mach. Learn. Res.* **2011**, *12*, 2825−2830.
(55) Scodeller, I.; De Oliveira Vigier, K.; Muller, E.; Ma, C.; Guégan, F.; Wischert, R.; Jérôme, F. A Combined Experimental-Theoretical Study on Diels-Alder Reaction with Bio-Based Furfural: Towards Renewable Aromatics. *ChemSusChem* **2020**, *14* (1), 313−323.
(56) Khan, T. S.; Gupta, S.; Ahmad, M.; Alam, M. I.; Haider, M. A. Effect of substituents and promoters on the Diels-Alder cycloaddition reaction in the biorenewable synthesis of trimellitic acid. *RSC Adv.* **2020**, *10* (51), 30656−30670.
(57) Rondestvedt, C. S.; Ver Nooy, C. D. Diels-Alder Reaction of Cinnamic Acid Derivatives with Cyclopentadiene. *J. Am. Chem. Soc.* **1955**, *77* (18), 4878−4883.
(58) Fisher, M. J.; Hehre, W. J.; Kahn, S. D.; Overman, L. E. Face selectivity in Diels-Alder reactions of chiral dienes containing allylic substituents. *J. Am. Chem. Soc.* **1988**, *110* (14), 4625−4633.
(59) Batatia, I.; Benner, P.; Chiang, Y.; Elena, A. M.; Kovács, D. P.; Riebesell, J.; Advincula, X. R.; Asta, M.; Avaylon, M.; Baldwin, W. J. A foundation model for atomistic materials chemistry. *arXiv preprint arXiv:2401.00096* **2023**, No. 2401.00096.
(60) Kovács, D. P.; Moore, J. H.; Browning, N. J.; Batatia, I.; Horton, J. T.; Kapil, V.; Witt, W. C.; Magdău, I.-B.; Cole, D. J.; Csányi, G. MACE-OFF23: Transferable machine learning force fields for organic molecules. *arXiv preprint arXiv:2312.15211* **2023**, No. 2312.15211.
(61) Kovács, D. P.; Batatia, I.; Arany, E. S.; Csányi, G. Evaluation of the MACE force field architecture: From medicinal chemistry to materials science. *J. Chem. Phys.* **2023**, *159* (4), No. 044118.
(62) Bannwarth, C.; Ehlert, S.; Grimme, S. GFN2-xTB—An Accurate and Broadly Parametrized Self-Consistent Tight-Binding Quantum Chemical Method with Multipole Electrostatics and Density-Dependent Dispersion Contributions. *J. Chem. Theory Comput.* **2019**, *15* (3), 1652−1671.
(63) Hermes, E. D.; Sargsyan, K.; Najm, H. N.; Zádor, J. Sella, an Open-Source Automation-Friendly Molecular Saddle Point Optimizer. *J. Chem. Theory Comput.* **2022**, *18* (11), 6974−6988.
(64) Stennett, T.; Mattock, J. D.; Pentecost, L.; Vargas, A.; Braunschweig, H. Chelated Diborenes and Their Inverse-Electron-Demand Diels-Alder Reactions with Dienes. *Angew. Chem. Int. Edit* **2018**, *57* (46), 15276−15281.
(65) Liu, F.; Paton, R. S.; Kim, S.; Liang, Y.; Houk, K. N. Diels-Alder Reactivities of Strained and Unstrained Cycloalkenes with Normal and Inverse-Electron-Demand Dienes: Activation Barriers and Distortion/Interaction Analysis. *J. Am. Chem. Soc.* **2013**, *135* (41), 15642−15649.
(66) Ramirez, M.; Svatunek, D.; Liu, F.; Garg, N. K.; Houk, K. N. Origins of Endo Selectivity in Diels-Alder Reactions of Cyclic Allene Dienophiles. *Angew. Chem. Int. Edit* **2021**, *60* (27), 14989−14997.
(67) Palasz, A.; Palasz, T. Knoevenagel condensation of cyclic ketones with benzoylacetonitrile and N, N'-dimethylbarbituric acid. Application of sterically hindered condensation products in the synthesis of spiro and dispiropyrans by hetero-Diels-Alder reactions. *Tetrahedron* **2011**, *67* (7), 1422−1431.
(68) Kopchuk, D. S.; Chepchugov, N. V.; Taniya, O. S.; Khasanov, A. F.; Giri, K.; Kovalev, I. S.; Santra, S.; Zyryanov, G. V.; Majee, A.; Rusinov, V. L.; et al. 3-Cyano-2-azaanthracene-based 'push-pull' fluorophores: A one-step preparation from 5-cyano-1,2,4-triazines and 2,3-dehydronaphthalene, generated in situ. *Tetrahedron Lett.* **2016**, *57* (50), 5639−5643.
(69) Surasani, S. R.; Parumala, S. K. R.; Peddinti, R. K. Diels-Alder reactions of 4-halo masked o-benzoquinones. Experimental and theoretical investigations. *Org. Biomol Chem.* **2014**, *12* (30), 5656−5668.

https://doi.org/10.1021/acsomega.5c02620
ACS Omega XXXX, XXX, XXX−XXX